

OPEN ACCESS

EDITED BY

Annalisa Chiavaroli.

University of Studies G. d'Annunzio Chieti and Pescara, Italy

REVIEWED BY

Tzu-Hurng Cheng, China Medical University, Taiwan

Kaiwei Cai,

Guangzhou University of Chinese Medicine,

China

*CORRESPONDENCE

Qin Zhang

zhangq1030@163.com

Ting-Ting Shen,

⊠ jessyshen72@sina.com

[†]These authors have contributed equally to this work and share first authorship

RECEIVED 28 August 2025 ACCEPTED 14 October 2025 PUBLISHED 03 November 2025

Wu J-X, Wu Y-L, Li M-F, Liu N, Liu Y, Huang Y-P, Gan Y, Wang X-Y, Chai H-S, Xu J, Xi Q, Guo X-R, Sheng H-M, Shen T-T and Zhang Q (2025) Multi-omics analysis elucidates the therapeutic mechanisms of the Quzhi formula in metabolic dysfunction-associated steatohepatitis targeting gut microbiota, lipid metabolism, and the role of its metabolite fraxin. Front. Pharmacol. 16:1694242. doi: 10.3389/fphar.2025.1694242

© 2025 Wu, Wu, Li, Liu, Liu, Huang, Gan, Wang, Chai, Xu, Xi, Guo, Sheng, Shen and Zhang. This is an open-access article distributed under the terms of the Creative Commons Attribution License (CC BY). The use, distribution or reproduction in other forums is permitted. provided the original author(s) and the copyright owner(s) are credited and that the original publication in this journal is cited, in accordance with accepted academic practice. No use, distribution or reproduction is permitted which does not comply with these

Multi-omics analysis elucidates the therapeutic mechanisms of the Quzhi formula in metabolic dysfunction-associated steatohepatitis targeting gut microbiota, lipid metabolism, and the role of its metabolite fraxin

Jiao-Xiang Wu^{1‡}, Yue-Lan Wu^{1‡}, Mei-Fang Li², Nian Liu³, Ying Liu⁴, Yan-Ping Huang¹, Yuan Gan¹, Xiao-Yu Wang¹, Hai-Sheng Chai⁵, Jin Xu¹, Qian Xi⁶, Xi-Rong Guo¹, Hui-Ming Sheng¹, Ting-Ting Shen (b) 1* and Qin Zhang (c) 1*

¹Phase I Clinical Trial Unit and Department of Infectious Diseases and Department of Clinical Laboratory and Plastic Surgery Department, Tongren Hospital, Shanghai Jiao Tong University School of Medicine, Shanghai, China, ²Henan University, Zhengzhou, China, ³eHealth Program of Shanghai Anti-doping Laboratory, Shanghai University of Sport, Shanghai, China, ⁴Clinical College of Traditional Chinese Medicine, Gansu University of Chinese Medicine, Lanzhou, China, ⁵Yueyang Integrated Chinese and Western Medicine Hospital, Shanghai University of Traditional Chinese Medicine, Shanghai, China, ⁶Department of Endocrinology, Shanghai Pudong New Area Gongli Hospital, Shanghai, China

Metabolic dysfunction-associated steatohepatitis (MASH) is an advanced stage of fatty liver disease with no approved pharmacotherapies. The Quzhi Formula (QZF), a traditional Chinese medicine utilized clinically for nearly two decades, has shown promising efficacy against MASH; however, its mechanisms of action remain largely unexplored. To elucidate these mechanisms, we conducted a multi-omics investigation integrating 16S rRNA sequencing, untargeted metabolomics, and transcriptomics in a MASH mouse model, with findings validated by histology. QZF treatment significantly alleviated hepatic steatosis, restored gut microbial diversity, and suppressed the proliferation of Enterococcus, a genus implicated in MASH pathogenesis. Transcriptomic and metabolomic analyses demonstrated that QZF's therapeutic effects were mediated through the regulation of lipid metabolic pathways and the activation of autophagy. Furthermore, we identified fraxin as a pivotal bioactive metabolite contributing to QZF-induced autophagy. Our study demonstrates that QZF ameliorates MASH in a concerted manner by remodeling the gut microbiota, reprogramming hepatic metabolism, and promoting autophagy via fraxin. These results provide a comprehensive mechanistic foundation for QZF as a multi-targeted therapeutic candidate for MASH.

KEYWORDS

metabolic dysfunction-associated steatohepatitis (MASH), Quzhi formula (QZF), fraxin, AMPK, autophagy

1 Introduction

Metabolic dysfunction-associated fatty liver disease (MAFLD), formerly known as non-alcoholic fatty liver disease (NAFLD), represents the predominant form of chronic liver disease worldwide, with its estimated prevalence having risen to 38.2% (Wong et al., 2023). Metabolic dysfunction-associated steatohepatitis (MASH), a distinct pathological subtype of MAFLD (Rao et al., 2023; Tamimi et al., 2024), is characterized as an inflammatory condition featuring simple hepatocellular steatosis, portal or central vein inflammatory cell infiltration, and hepatocyte ballooning (Hags et al., 2024; Wu et al., 2021; Qu et al., 2019). As the advanced stage of the MAFLD disease spectrum, MASH progresses to hepatic fibrosis in 40.76% of cases and drives a marked increase in cirrhosis prevalence (Miao et al., 2024). It is projected to surpass viral hepatitis as the primary indication for liver transplantation and the leading etiology of hepatocellular carcinoma in the future (Younossi et al., 2025). Furthermore, MASH-associated metabolic dysregulation correlates with elevated risks of severe latestage hepatic complications (Jarvis et al., 2020). Currently, only one FDA-approved therapeutic agent for MASH is available (Kokkorakis et al., 2024), leaving the substantial medical need for preventing, halting, or reversing MASH largely unmet.

Emerging evidence underscores MAFLD as a multifactorial disorder arising from systemic metabolic dysregulation across organ systems. Central to its pathogenesis are interconnected risk factors including hepatic nutrient overload (particularly carbohydrates/lipids), accumulation of lipotoxic metabolites, oxidative stress, immune activation, endoplasmic reticulum stress, and genetic predisposition (Buzzetti et al., 2016; Younossi et al., 2018). This complexity manifests through a "multiple-hit" pathological framework characterized by hepatocellular lipid accumulation, insulin resistance, oxidative DNA damage, inflammatory cascades, and fibrotic remodeling (Kuchay et al., 2020). Gut microbiota dysbiosis is intricately linked to the pathogenesis of MASH. Under the synergistic influence risk factors of environmental and genetic predisposition, crosstalk among the liver, adipose tissue, and gut microbiota drives systemic metabolic dysfunction and insulin resistance, resulting in enhanced hepatic fatty acid influx and de novo lipogenesis (Leung et al., 2016). Furthermore, autophagy—a conserved cellular degradation pathway enabling the recycling of proteins and organelles—has emerged as a critical regulator in MASH progression (Ren et al., 2024).

Recent studies have shown that traditional Chinese medicine can be used as a potential drug for the treatment of MASH (Liang et al., 2025; Xu et al., 2024; Gong et al., 2022; Tang et al., 2024), such as the *Xiaoji-chenpi* formula (XCF) can improve lipid metabolism,

Abbreviations: MASH, metabolic dysfunction-associated steatohepatitis; QZF, Quzhi formula; MAFLD, metabolic dysfunction-associated fatty liver disease; NAFLD, non-alcoholic fatty liver disease; TCM, traditional chinese medicinal; CDAHFD, choline-deficient, I-amino acid-defined, high-fat diet; OA, Oleic acid; PA, Palmitic acid; GSEA, Gene Set Enrichment Analysis; OPLS-D, Orthogonal partial least squares discriminant analysis; FFA, free fatty acid; TC, total cholesterol; TG, triglyceride; LPS, lipopolysaccharides; MCD, methionine-choline-deficient; VLDL, very-low-density lipoprotein; ERS, endoplasmic reticulum stress.

inhibite inflammation, and reduce liver fibrosis in MAFLD (Liang et al., 2025). Gan-jiang-ling-zhu decoction improves steatohepatitis by regulating gut microbiota-mediated 12-tridecenoic acid inhibition (Xu et al., 2024). The Quzhi Formula (QZF), a traditional Chinese medicine, emerges here as a further potential therapeutic for metabolic dysfunction-associated steatohepatitis (MASH). This clinically optimized formulation has been systematically employed in our therapeutic practice for nearly two decades, demonstrating consistent and significant clinical efficacy in disease management (Xie et al., 2010; Chai et al., 2020; Wu et al., 2022). The QZF is composed of three medicinal botanicals: Polygonum cuspidatum Siebold and Zucc. (Hu zhang), Senna obtusifolia (L.) H. S. Irwin and Barneby (Jue mingzi), and Crataegus pinnatifida Bunge (Shan zha) (Wu et al., 2022). Polygonum cuspidatum Siebold and Zucc, serving as the sovereign botanical drug in this formulation, contains multiple bioactive metabolites-including quinones, stilbenes, and flavonoids-that exert multifaceted therapeutic effects on hyperlipidemia, inflammatory cascades, microbial infections, and oncogenesis through distinct pharmacological mechanisms (Peng et al., 2013). Senna obtusifolia (L.) H. S. Irwin and Barneby, another critical botanical drug, demonstrates broad-spectrum bioactivities encompassing antidiabetic, anti-inflammatory, antineoplastic, antimutagenic, and hepatoprotective properties (Yadav et al., 2010). Meanwhile, C. pinnatifida Bunge is extensively documented in both preclinical and clinical contexts for its efficacy in modulating metabolic syndrome-related pathways (Dehghani et al., 2019).

AMP-activated protein kinase (AMPK) serves as a central regulator of cellular energy metabolism and represents a critical therapeutic target for MASH intervention (Wang et al., 2025). And many natural bioactive metabolites demonstrate promising potential for the treatment of MASH by regulating AMPK pathway. In this study, we demonstrate that both QZF and Fraxin also activate AMPK and ameliorate lipid accumulation in vitro.

Collectively, QZF is rationally designed based on the pathophysiological characteristics of MASH, integrating optimized phytochemical synergies to target multifactorial disease mechanisms. In this study, integrated multi-omics analyses reveal that QZF alleviates MASH by modulating the gut-liver axis to restore microbial diversity, suppress pro-steatotic *Enterococcus*, and activate autophagy-driven metabolic reprogramming, thereby reducing hepatic lipid accumulation and positioning QZF as a systems-level therapeutic for metabolic disorders.

2 Materials and methods

2.1 Botanical drugs materials and extracts preparation

2.1.1 Botanical drugs and authentication

The botanical drugs in QZF are detailed in Table 1, which includes their scientific and species names, pharmaceutical names, Chinese phonetic names, and origins. The formula consists of three botanical drugs: *P. cuspidatum* Siebold and Zucc. (20 g), *S. obtusifolia* (L.). H. S. Irwin and Barneby (30 g), and *C.*

TABLE 1 The botanical drug(s) of QZF.

Scientific name	Pharmaceutical name	Latin name	Chinese pin yin	Place of origin (commercial supplier/province)
Senna obtusifolia (L.) H. S. Irwin and Barneby	Sickle Senna Seed	Cassiae Semen	Jue mingzi	Shanghai Wanshicheng Pharmaceutical Co., Ltd. (Shanghai, China)
Polygonum cuspidatum Siebold and Zucc.	Giant Knotweed Root	Polygoni Cuspidati Rhizoma et Radix	Hu zhang	Shanghai Kangqiao Chinese MedicineTablet Co., Ltd. (Shanghai, China)
Crataegus pinnatifida Bunge	Chinese Hawthorn Fruit	Crataegi Fructus	Shan zha	Shanghai Kangqiao Chinese MedicineTablet Co., Ltd. (Shanghai, China)

TABLE 2 16S sequence related primer information.

Туре	Region	Primer name	Primer sequence	Product length
168	V4	515F	GTGYCAGCMGCCGCGGTAA	~292
		806R	GGACTACNVGGGTWTCTAAT	
168	V3-V4	341F	CCTACGGGNGGCWGCAG	~466
		806R	GGACTACHVGGGTATCTAAT	
168	V4-V5	515F	GTGCCAGCMGCCGCGGTAA	~412
		907R	CCGTCAATTCCTTTGAGTTT	
168	V5-V7	799F	AACMGGATTAGATACCCKG	~414
		1193R	ACGTCATCCCCACCTTCC	
16S V4-V5	V4-V5	Arch519F	CAGCMGCCGCGGTAA	~416
		Arch915R	GTGCTCCCCGCCAATTCCT	
18S	V4	528F	GCGGTAATTCCAGCTCCAA	~260
		706R	AATCCRAGAATTTCACCTCT	

pinnatifida Bunge (30 g). These botanical drugs were sourced from the Shanghai Wanshicheng Pharmaceutical Co., Ltd., (Shanghai, China) or Shanghai Kangqiao Chinese MedicineTablet Co., Ltd., (Shanghai, China) and authenticated by professor Wei Liu, Department of Pharmacy, Shanghai University of Traditional Chinese Medicine.

The voucher specimen of P. cuspidatum Siebold and Zucc (Huzhang) is deposited in the Herbarium of the College of Pharmacy, Guizhou University of Traditional Chinese Medicine (Guizhou, China), with the voucher number GZTM0094265. It was collected and preserved by Hou Xiaoqi on 12 June 2019, in Guizhou, China. The specimen of S. obtusifolia (L.) H. S. Irwin and Barneby (Juemingzi) is housed in the Plant Herbarium of the School of Geography and Environmental Science, Guizhou Normal University (Guizhou, China), under the voucher number GNUG0008259. It was collected and preserved by Wang Yuanhong on 22 November 2017, in Guizhou, China. The specimen of C. pinnatifida Bunge (Shanzha) is stored in the Medicinal Plant Herbarium of the College of Pharmacy, Jiamusi University (Heilongjiang, China), with the voucher number JMSMC0005742. It was collected and preserved by Wang Lihong on 17 June 2023, in Heilongjiang, China.

2.1.2 Botanical drugs extract preparation

According to the specified ratio, 260 g of *P. cuspidatum* Siebold and Zucc., 390 g of *S. obtusifolia* (L.) H. S. Irwin and Barneby and 390 g of *C. pinnatifida* Bunge were taken. For the first extraction, 10 times the amount of water was added, and reflux extraction was performed for 2 h. For the second extraction, 8 times the amount of water was added, and reflux extraction was conducted for 1 h. The extract was filtered through a 200-mesh sieve, and the filtrate was concentrated to a relative density of 1.07, yielding approximately 1.825 kg. Under gentle stirring, 3.118 kg of ethanol was added to achieve an alcohol concentration of 60%. The mixture was then purified by standing for over 12 h. The supernatant was collected and concentrated to approximately 500 mL (density 1.154). This concentration was used for subsequent mass spectrometry analysis and animal administration.

2.1.3 Chemical profiling and quality control of QZF

To identify the metabolites of QZF extract, we performed LC-MS/MS, the results were presented in Supplementary Table S1. The LC-MS fingerprint of the QZF extract was established by identifying characteristic peaks in both positive and negative ion modes as described by Fan et al. (2022). The peak areas were recorded, and the relative standard deviations (RSD) for the relative retention time and

TABLE 3 Antibody used for western blot.

Protein	Manufacturer	Product number	Source
ASK1	CST	3762S	Rabbit
Phospho-JNK	proteintech	80024-1-RR	Rabbit/IgG
JNK	proteintech	66210-1-Ig	Mouse/ IgG1
P62/SQSTM1	proteintech	18420-1-AP	Rabbit/IgG
BAX	proteintech	50599-2-Ig	Rabbit/IgG
Bcl2	proteintech	26593-1-AP	Rabbit/IgG
LC3B	proteintech	18725-1-AP	Rabbit/IgG
ATG7	proteintech	10088-2-AP	Rabbit/IgG
NRF2	CST	12721S	Rabbit/IgG
АМРКα	CST	2532S	Rabbit/IgG
ΑΜΡΚβ1/2	CST	4150S	Rabbit/IgG
Phospho- AMPKα	CST	2535S	Rabbit/IgG

TABLE 4 RT-PCR primer sequences.

Gene	Primer	Sequence
ASK1	Forward	5'-CTGCATTTTGGGAAACTCGACT-3'
ASK1	Reverse	5'-AAGGTGGTAAAACAAGGACGG-3'
P62	Forward	5'-GACTACGACTTGTGTAGCGTC-3'
P62	Reverse	5'-AGTGTCCGTGTTTCACCTTCC-3'
Actin	Forward	5'-TTGTTACAGGAAGTCCCTTGCC-3'
Actin	Reverse	5'-ATGCTATCACCTCCCCTGTGTG-3'
GAPDH	Forward	5'-GTCAAGGCTGAGAACGGGAA-3'
GAPDH	Reverse	5'-AAATGAGCCCCAGCCTTCTC-3'

relative peak area were calculated as 0.00%–0.22% and 1.06%–1.43%, respectively, indicating good instrument precision. The cosine similarity algorithm was applied to calculate the similarity between all samples and the common peaks established based on all samples. Detailed fingerprint similarity results among samples can be found in the inter-sample similarity analysis table. Meanwhile, the cosine similarity algorithm was also used to compute the similarity between all samples and the common peaks established within different sample groups. These corresponding results are provided in Supplementary Figure S1 and the ConPhyMP-checklist were presented in Supplementary Table S2.

2.2 MASH model induction and QZF administration

As we described in 2022 (Wu et al., 2022), six-week-old male C57BL/6J mice (n = 45) were used for all experiments. MASH was

induced by feeding mice a choline-deficient, l-amino acid-defined, high-fat diet (CDAHFD, Dyets, CD-HF60) 11,12 for 3 weeks. Mice were randomly assigned to five groups: control (normal chow, n = 9), model (MASH, n = 9), QZF8.3331 g/kg -treated (MASH + QZF, n = 9), QZF4.1666 g/kg -treated (MASH + QZF, n = 9), and QZF-toxicity (normal chow + QZF 8.3331 g/kg, n = 9).

QZF was administered orally at a dose of 8.3331 g/kg/day or 4.1666 g/kg/day for 4 weeks following the establishment of the MASH model. The composition and dosage were based on previous clinical and pharmacological studies.

The mice were then sacrificed, and intestinal contents and liver samples were collected for analysis. Anesthesia was induced via intraperitoneal injection of 0.3% pentobarbital sodium at a dosage of 0.05 g/kg. Then the blood and liver samples were collected. All animal experiments were conducted in accordance with institutional ethical guidelines.

2.3 Liver tissue histological and lipid staining

Hepatic tissue specimens underwent immersion-fixation in 4% paraformaldehyde (24 h), followed by standard paraffin embedding procedures. Thin sections (5 μm) were prepared and subjected to hematoxylin and eosin (H&E) staining protocol to enable microscopic morphological analysis. Frozen liver sections prepared at $-20~^{\circ}\mathrm{C}$ cryostat temperature underwent Oil Red O staining (0.3% working solution, 37 $^{\circ}\mathrm{C}$ incubation) for specific detection of lipid deposits. Images were captured using a brightfield microscope.

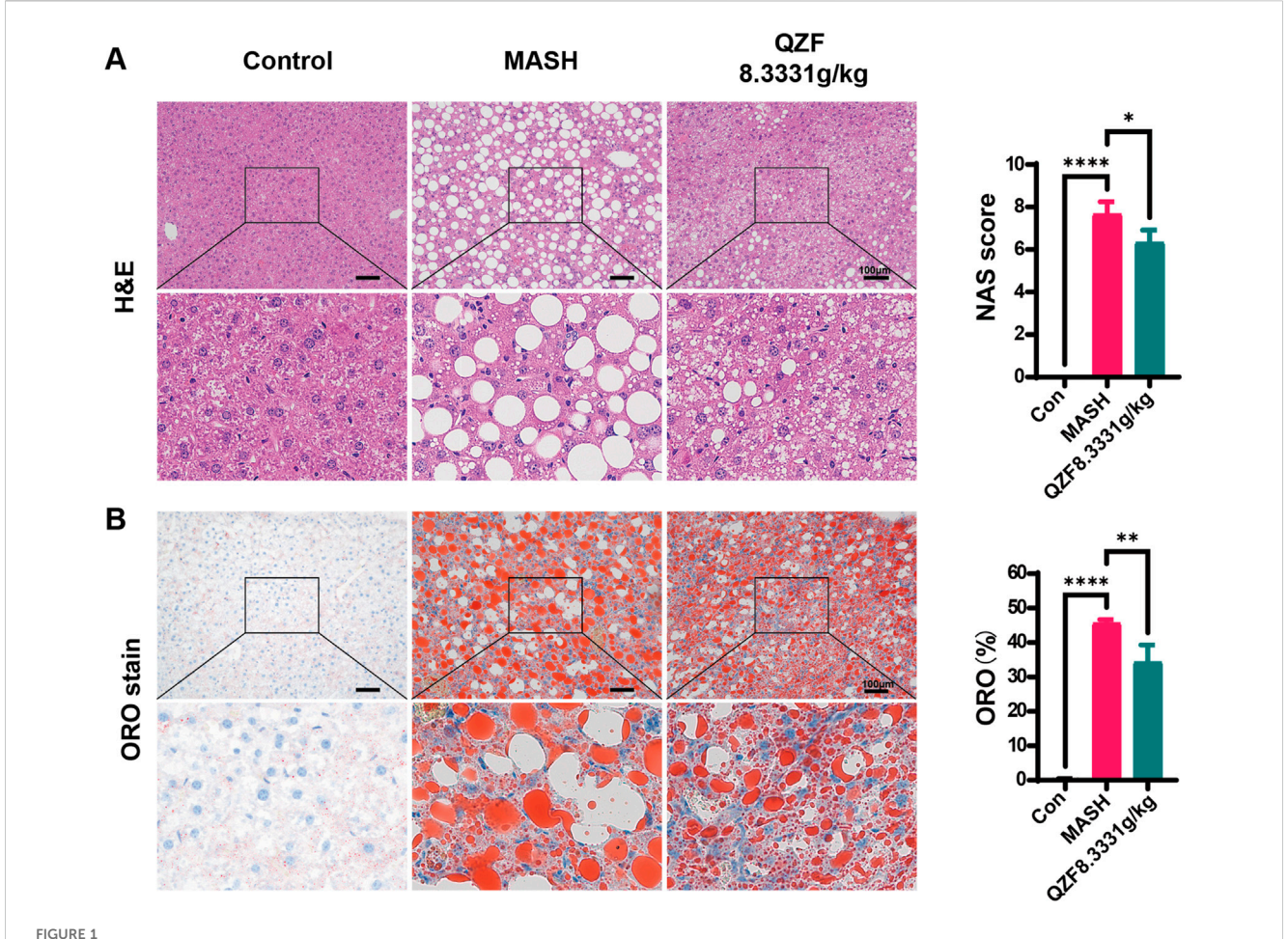
2.4 Gut microbiota analysis by 16S rRNA sequencing

Fecal samples were collected and subjected to microbial DNA extraction using the HiPure Soil DNA Kit or HiPure Stool DNA Kit (Magen, Guangzhou, China) in accordance with the manufacturer's protocols. The 16S rDNA hypervariable regions of the ribosomal RNA gene were amplified via polymerase chain reaction (PCR). The primers used were listed in Table 2. Each 50 μL PCR mixture contained 10 μL of $5\times$ Q5° Reaction Buffer, 10 μL of $5\times$ Q5° High GC Enhancer, 1.5 μL of 2.5 mM dNTPs, 1.5 μL of each primer (10 μM), 0.2 μL of Q5° High-Fidelity DNA Polymerase, and 50 ng of template DNA. All PCR reagents were obtained from New England Biolabs (USA).

The resulting amplicons were excised from 2% agarose gels and purified with the AxyPrep DNA Gel Extraction Kit (Axygen Biosciences, Union City, CA, USA) following the manufacturer's instructions. The purified products were quantified using the ABI StepOnePlus Real-Time PCR System (Life Technologies, Foster City, USA). Equimolar amounts of the amplicons were pooled and subjected to paired-end sequencing (PE250) on an Illumina platform according to standard protocols. Sequencing data were subsequently analyzed with QIIME2 and LEfSe to assess microbial diversity, relative abundance, and identify potential biomarkers.

2.5 Untargeted metabolomics analysis

Liver tissues were harvested, homogenized, and extracted using methanol/acetonitrile mixtures. Metabolomic profiling was



OZF alleviated hepatic steatosis in MASH mice. Male C57BL/6 SPF mice (6 weeks old) were maintained on CDAHFD for 3 weeks and subsequently administered the OZF (8.3331 g/kg) or PBS vehicle by daily gavage for 4 weeks. At the end of week 7, mice were euthanized and liver samples were obtained. Liver sections subjected to (A) H6E or (B) Oil Red O staining are shown representatively. NAFLD Activity Score (NAS) and representative Oil Red O-stained liver sections with corresponding semi-quantitative analysis of lipid deposition performed using ImageJ. **p < 0.01, ***p < 0.001, ***p < 0.001vs. model group (one-way ANOVA). Abbreviation: MASH, metabolic associated steatohepatitis; CDAHFD, choline-deficient, I-amino acid-defined, high-fat diet; H6E, hematoxylin and eosin.

performed using UHPLC-Q-TOF-MS under both positive and negative ion modes. Analysis was performed using an UHPLC (1290 Infinity LC, Agilent Technologies) coupled to a quadrupole time-of-flight (AB Sciex TripleTOF 6600) in Shanghai Applied Protein Technology Co., Ltd. For HILIC separation, samples were analyzed using a 2.1 mm \times 100 mm ACQUIY UPLC BEH 1.7 μm column (waters, Ireland). For RPLC separation, a 2.1 mm \times 100 mm ACQUIY UPLC HSS T3 1.8 μm column (Waters, Ireland) was used. Data were processed with XCMS and annotated against the HMDB and KEGG databases. Multivariate statistical analyses (PCA, OPLS-DA) were conducted to identify differential metabolites and enriched pathways.

2.6 RNAseq of liver tissue

Total liver RNA was isolated from hepatic tissues using Trizol reagent. RNA quantification was precisely determined using Qubit 4.0 Fluorometer. After rigorous quality control, strand-specific transcriptome libraries were prepared following Illumina TruSeq

Stranded mRNA protocol and sequenced on Illumina Novaseq 6000 platform with paired-end 150 bp (PE150) configuration, generating raw sequencing data in FASTQ format. Differentially expressed genes were defined by fold change >1.5 and p <0.05, and subjected to GO and KEGG enrichment analysis.

2.7 Cell viability measurement

AML12 cells were incubated in AML12 Cell Specific Medium (Wuhan Pricella Biotechnology, CM-0602) with or without various concentrations of Fraxin (TargetMol, USA, T3783) for 24 h. The cell viability was detected using CCK-8 assay kit (TargetMol, USA, C0005) as the manufacture's instruction.

2.8 Cell Oil Red O staining

To evaluate the intracellular lipid accumulation, Cell Oil Red O Staining was performed. HepG2 cells were first treated with $100~\mu M$

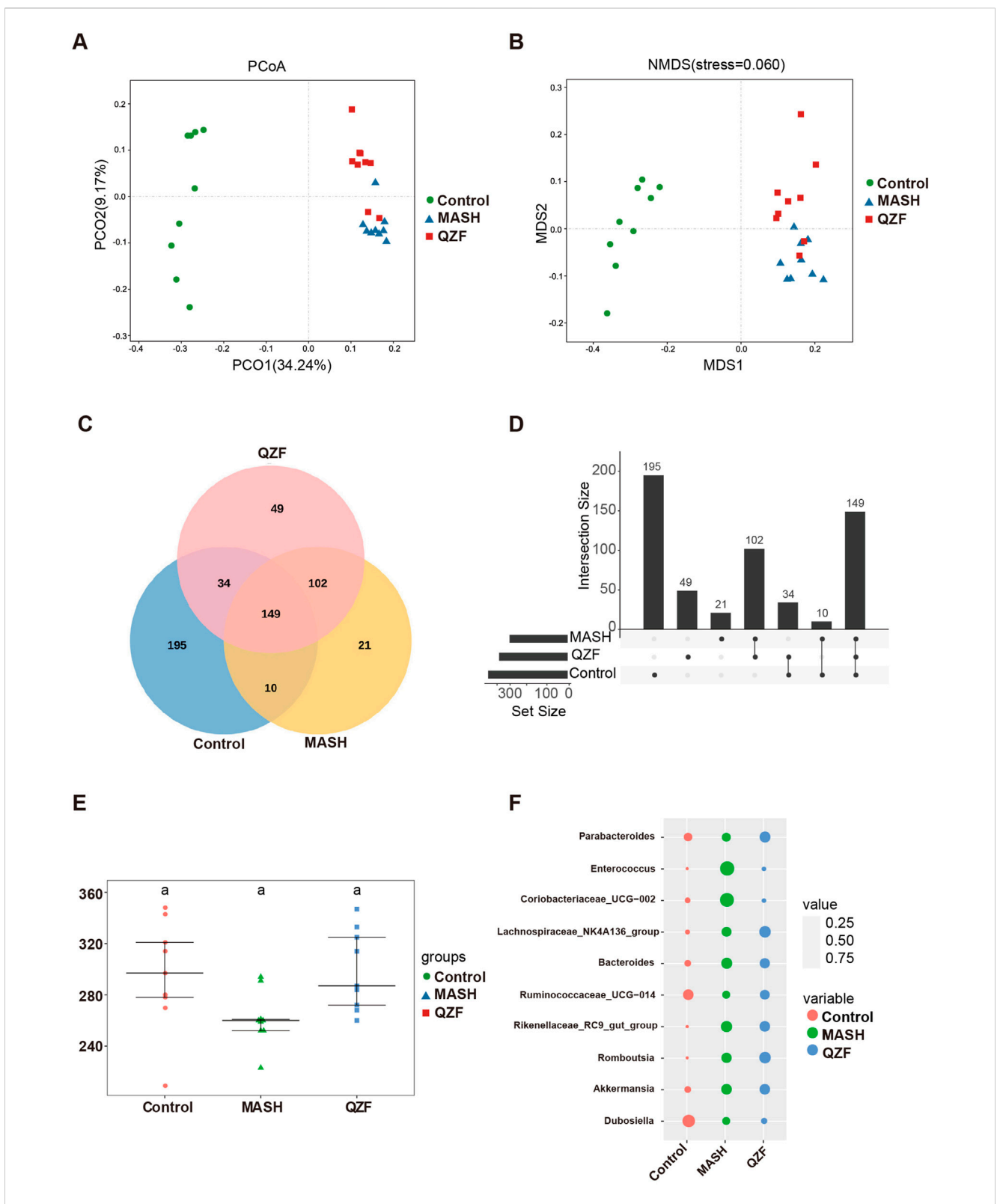
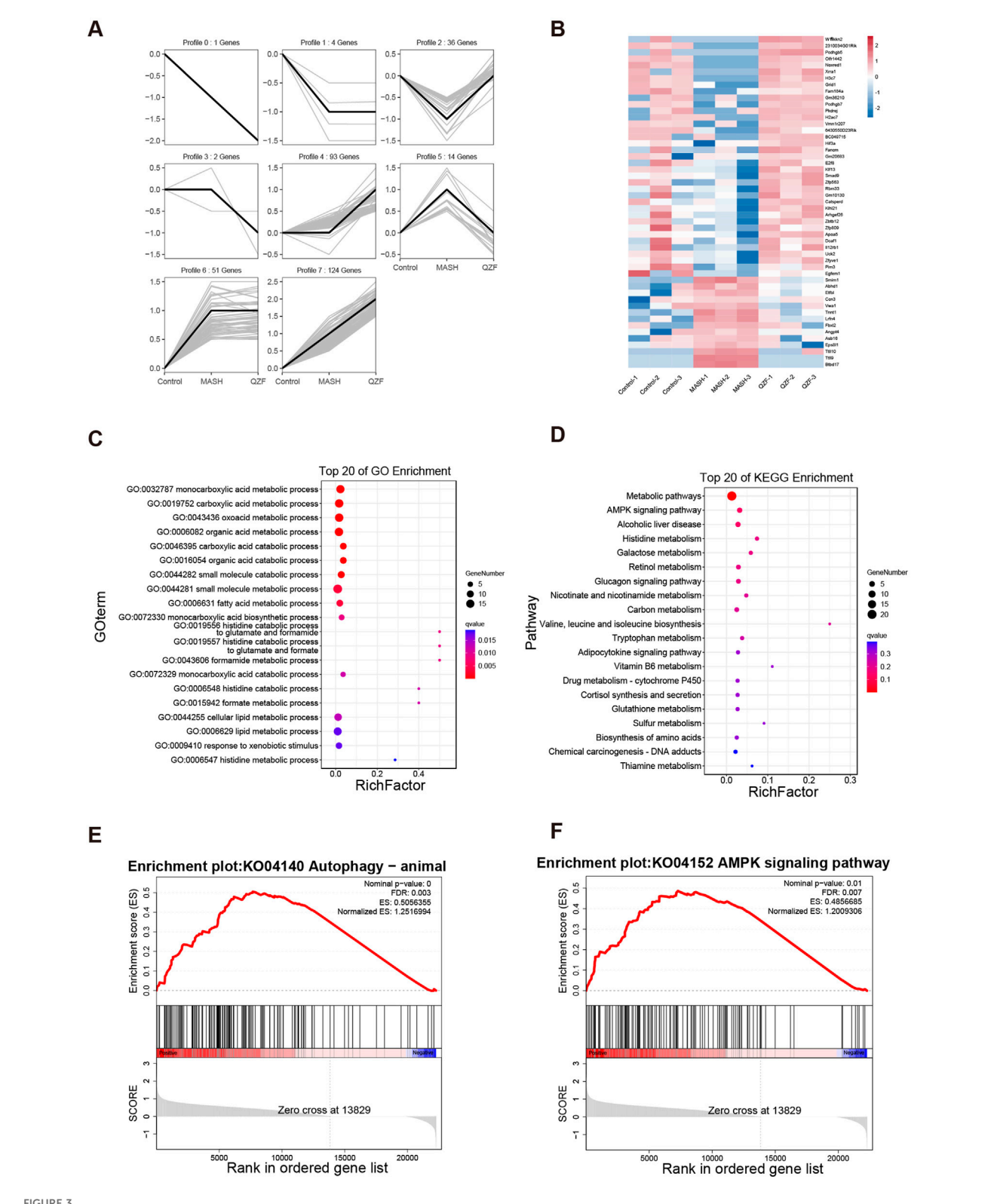
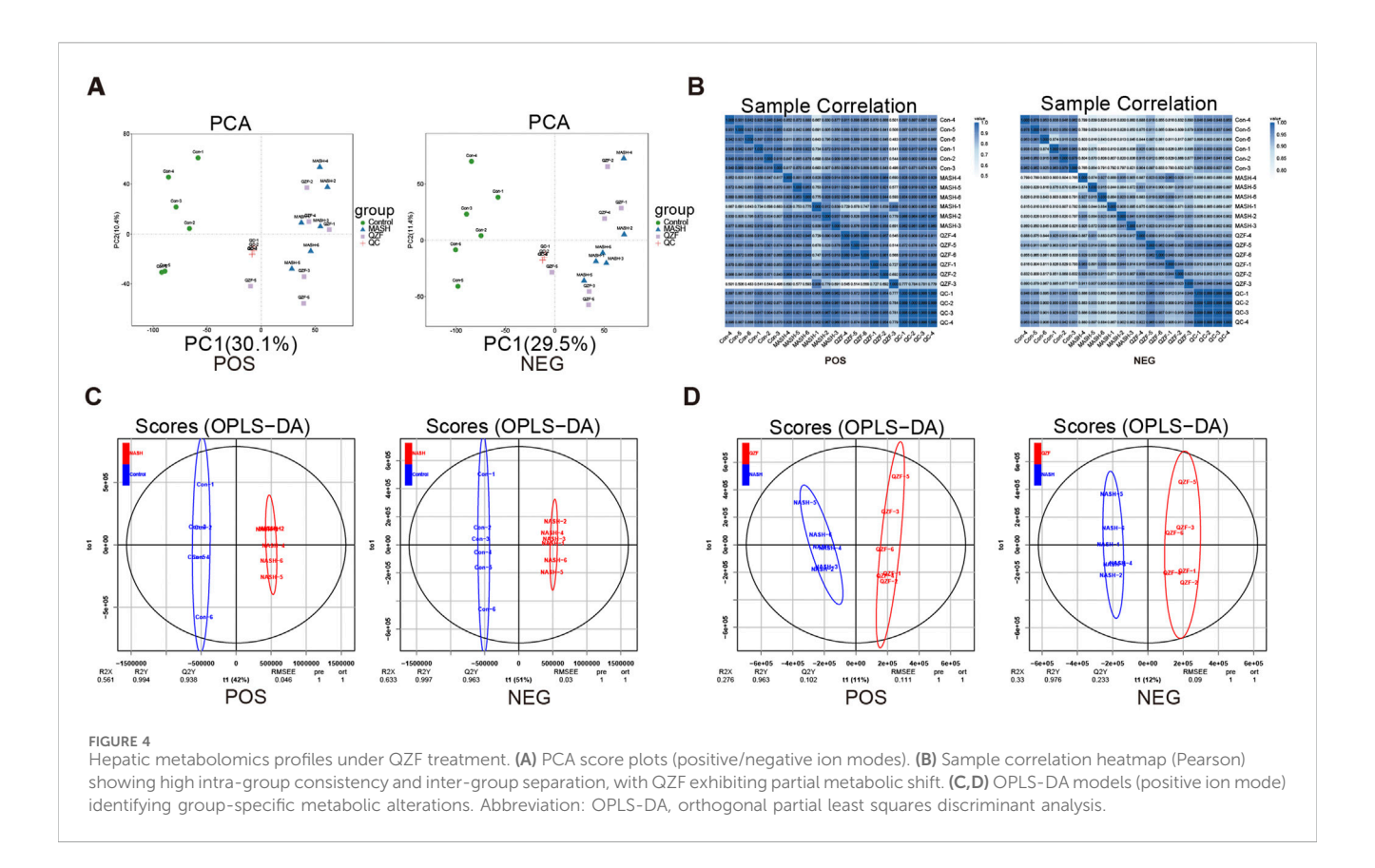


FIGURE 2

QZF improves microbial diversity and composition in MASH mice. (A) Principal coordinate analysis (PCoA) and (B) non-metric multidimensional scaling (NMDS) plots, both based on Bray-Curtis dissimilarity, illustrate distinct clustering patterns between the QZF-treated and vehicle-control groups. (C) Venn diagram and (D) UpSet plot depicting shared and unique bacterial OTUs across Control, MASH, and QZF groups. (E) Alpha diversity (observed OTU counts) across Control, MASH, and QZF groups. (F) Differential abundance of MAFLD-associated genera revealed by taxonomic profiling.



OZF Modulates Hepatic Transcriptome and Activates AMPK/Autophagy-Related Metabolic Pathways. RNA-seq analysis of QZF mechanisms in MASH. (A) Gene clustering into eight profiles based on expression trends across Control, MASH and QZF groups. (B) Reversion of Profiles 2 and 5 to normal transcriptional states post-QZF treatment. (C,D) Metabolic pathway enrichment via GO and KEGG analyses. (E,F) GSEA showing enrichment of autophagy and AMPK signaling pathway in QZF group.



Oleic acid (OA) and 50 μM Palmitic acid (PA), followed by 24 h coexposure to Fraxin at 40 or 60 μM concentrations, with 10 μM resmetirom serving as the positive control. HepG2 cells were fixed in 4% paraformaldehyde for 0.5 h and stained by Oil Red O solution for 0.5 h. Oil red O stained hepatocytes were rinsed with 60% isopropanol and counterstained with hematoxylin. After being washed with distilled water, the stained lipid droplets within cells were observed under an inverted microscope.

2.9 BODIPY 493 staining

HepG2 cells were fixed with 4% paraformaldehyde (15 min) and subsequently stained with BODIPY 493 fluorescent dye (20 min incubation). Following three PBS washes to remove unbound probes, intracellular lipid droplets were visualized under a fluorescence microscope, with image acquisition performed using consistent exposure parameters across experimental groups.

2.10 Cell lipid measurement

AML12 cells were first exposed to $100~\mu M$ OA and $50~\mu M$ PA for 24 h, followed by 24-h treatment with Fraxin at graded concentrations (40 and 60 μM) or 10 μM Resmetirom. Subsequently, cellular lysates were collected by centrifugation. Hepatic lipid profiles were quantified using commercially available enzymatic assay kits (Total Cholesterol: A111-2-1; Triglycerides: A110-2-1, Nanjing Jiancheng Bioengineering

Institute) according to the manufacturer's protocols, with optical density measurements normalized to total protein content.

2.11 Western blot

Cellular samples were homogenized with ice-cold RIPA lysis buffer (Thermo Scientific, Cat# 89900) containing protease/phosphatase inhibitor to extract the total proteins. Then, the extracted protein samples were separated using 10% SDS-PAGE and transferred onto polyvinylidene fluoride (PVDF, Millipore, IPVH00010) membranes. After blocking with 5% non-fat milk, the membranes were incubated with primary antibodies (Table 3) at 4 °C overnight. Following incubated corresponding secondary antibodies for 2 h at room temperature, the protein bands were visualized using Omni ECL reagent (EpiZyme, SQ101 or SQ201).

2.12 qPCR

The total RNA was extracted from liver or hepatocytes with Trizol reagent (Sangon Biotech, B511311-0100), following the manufacturer's instruction. The cDNA synthesis was performed using a reverse transcriptase kit (Takara, RR047). The mRNA levels of genes involved in inflammation and Lipid metabolism were estimated by RT-PCR using an SYBR Green qPCR Master Mix kit (Takara, RR820B). The primer sequences used to amplify mRNA were shown in Table 4.

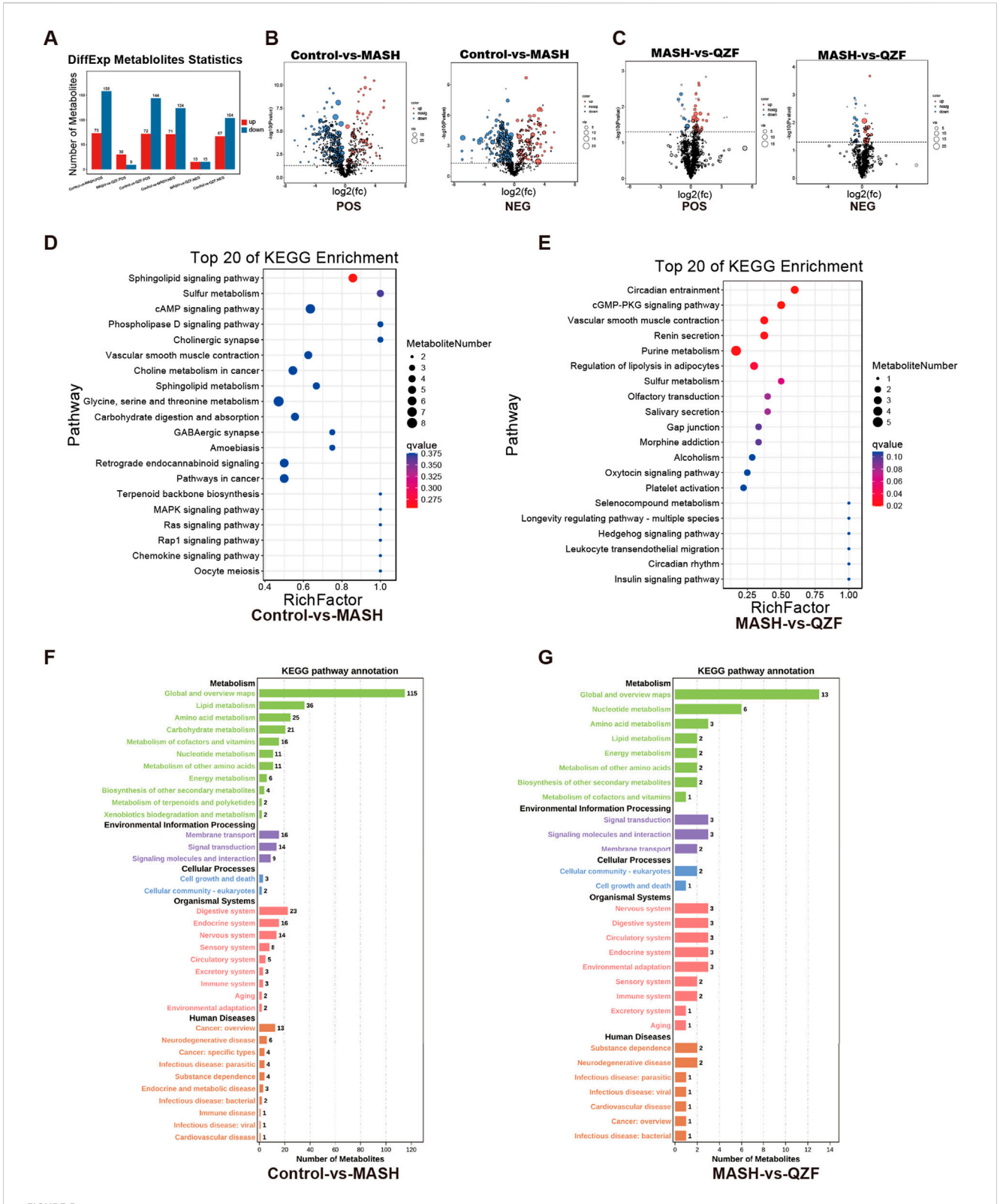
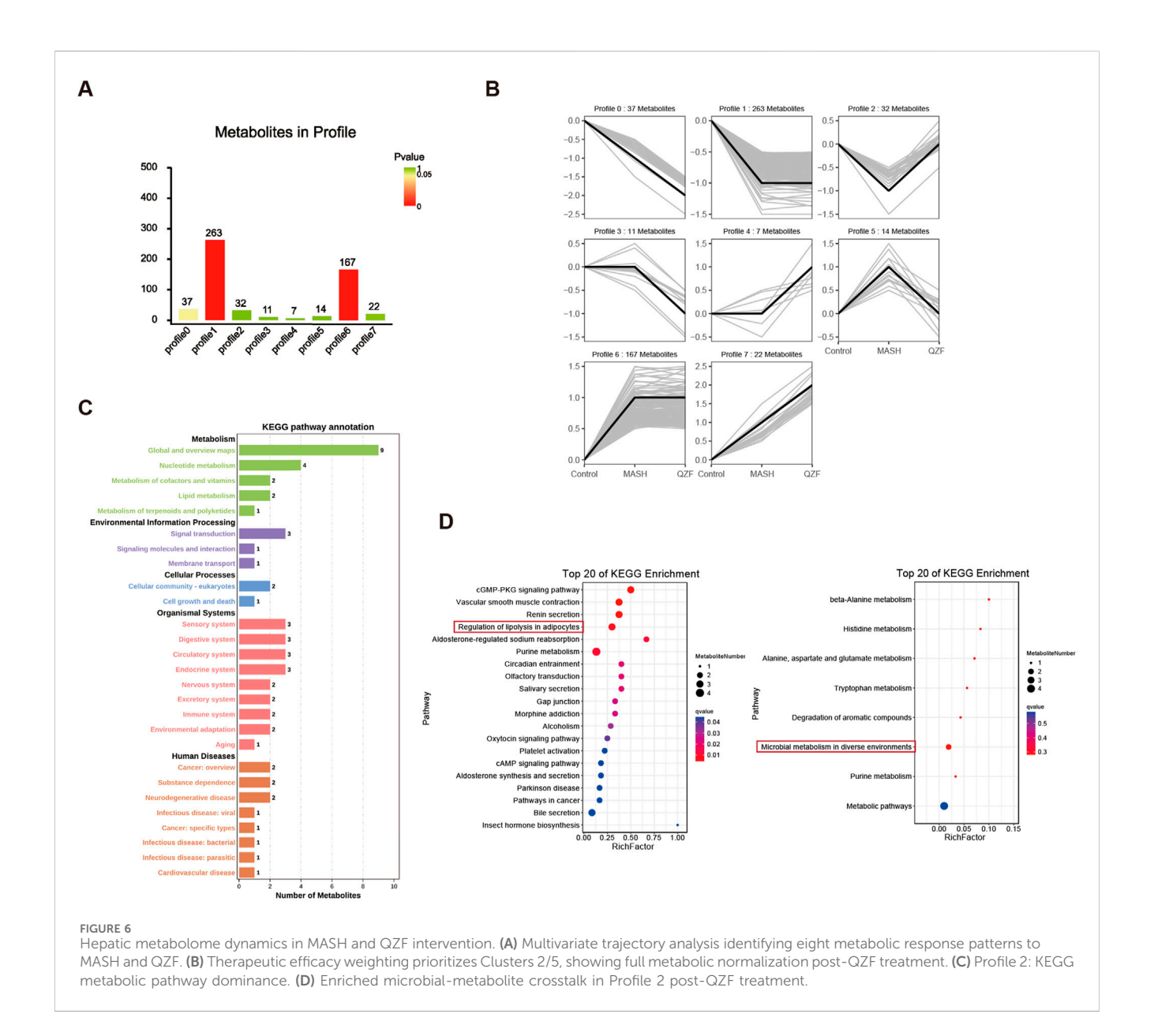


FIGURE 5
Key metabolic pathways altered by QZF. (A–C) Volcano plots demonstrate severe metabolic dysregulation in MASH versus Control with 231 significantly altered metabolites (73 upregulated, 158 downregulated), contrasted by only 39 differential metabolites in MASH versus QZF-treated groups, indicating therapeutic metabolic reset; (D–G) Subsequent pathway enrichment analysis (KEGG).



2.13 Molecular docking

The three-dimensional structures of core autophagy pathway targets were retrieved from the UniProt database (https://www.uniprot.org/). The three-dimensional structure of Fraxin was obtained from the PubChem database (https://pubchem.ncbi.nlm.nih.gov/). Protein structures were prepared using PyMOL software, involving hydrogen addition, water removal, and ligand separation. Grid box parameters were optimized in AutoDock Tools. Molecular docking simulations were subsequently performed using AutoDock Vina to quantitatively assess the binding modes between the small molecule drug and the core targets. The resulting docking poses were visualized using PyMOL.

2.14 Statistical analysis

Data were expressed as mean \pm SEM. Comparisons between groups were performed using one-way ANOVA followed by Tukey's

post hoc test. Statistical significance was set at p < 0.05. All analyses were performed using GraphPad Prism and R software.

3 Results

3.1 QZF remodeled gut microbiota composition in MASH mice

The therapeutic potential of the QZF was evaluated in a mouse model of MASH induced by a CDA-HFD diet. Treatment with the high dose of QZF (8.3331 g/kg) significantly alleviated hepatic steatosis and markedly attenuated lipid-associated inflammation compared to the model group (Figures 1A,B). Although the low-dose QZF group (4.1666 g/kg) showed a trend toward improvement, the effect did not reach statistical significance (Supplementary Figure S2). Furthermore, a dedicated acute toxicity study confirmed that the high-dose QZF regimen was well-tolerated, showing no signs of

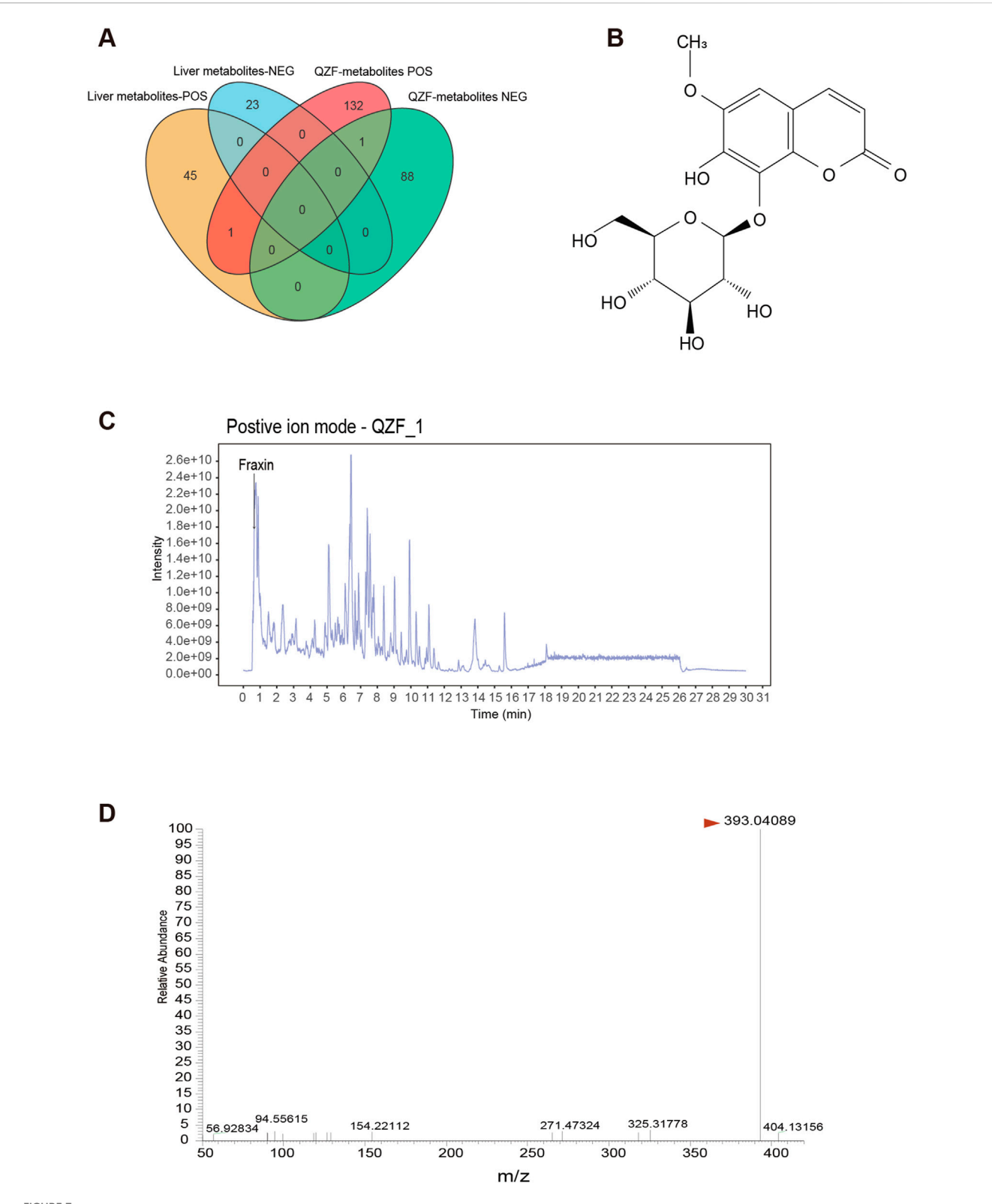


FIGURE 7
Identification of Fraxin from QZF Extract as a Bioavailable Agent Targeting Hepatic Therapeutic Clusters. (A) Venn diagram identifying 2 QZF-derived metabolites overlapping with in vivo therapeutic clusters (Profile2/5), suggesting systemic bioavailability. (B) Chemical structural formula of Fraxin. (C) LC-MS chromatograms confirming consistent detection of Fraxin in QZF extract.

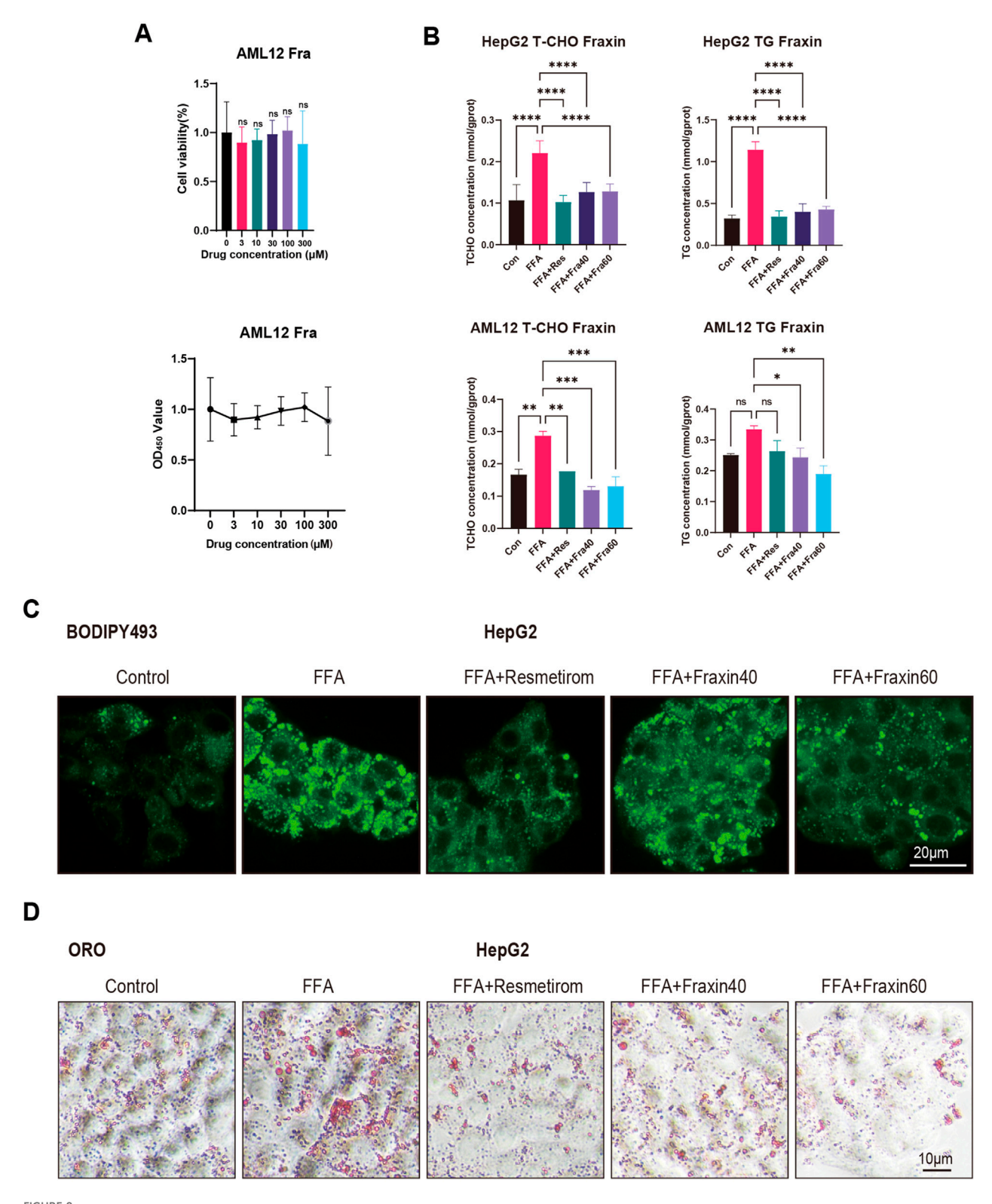


FIGURE 8 Fraxin ameliorates hepatic steatosis *in vitro.* (A) Cell viability assay: No cytotoxicity in AML12 hepatocytes across Fraxin doses (0–120 μ M). (B) Biochemical quantification: Fraxin dose-dependently decreases TC/TG in FFA-induced HepG2/AML12 steatosis models (P < 0.01 vs. FFA). (C,D) BODIPY/Oil Red O staining shows Fraxin (60 μ M) abolishes lipid accumulation.

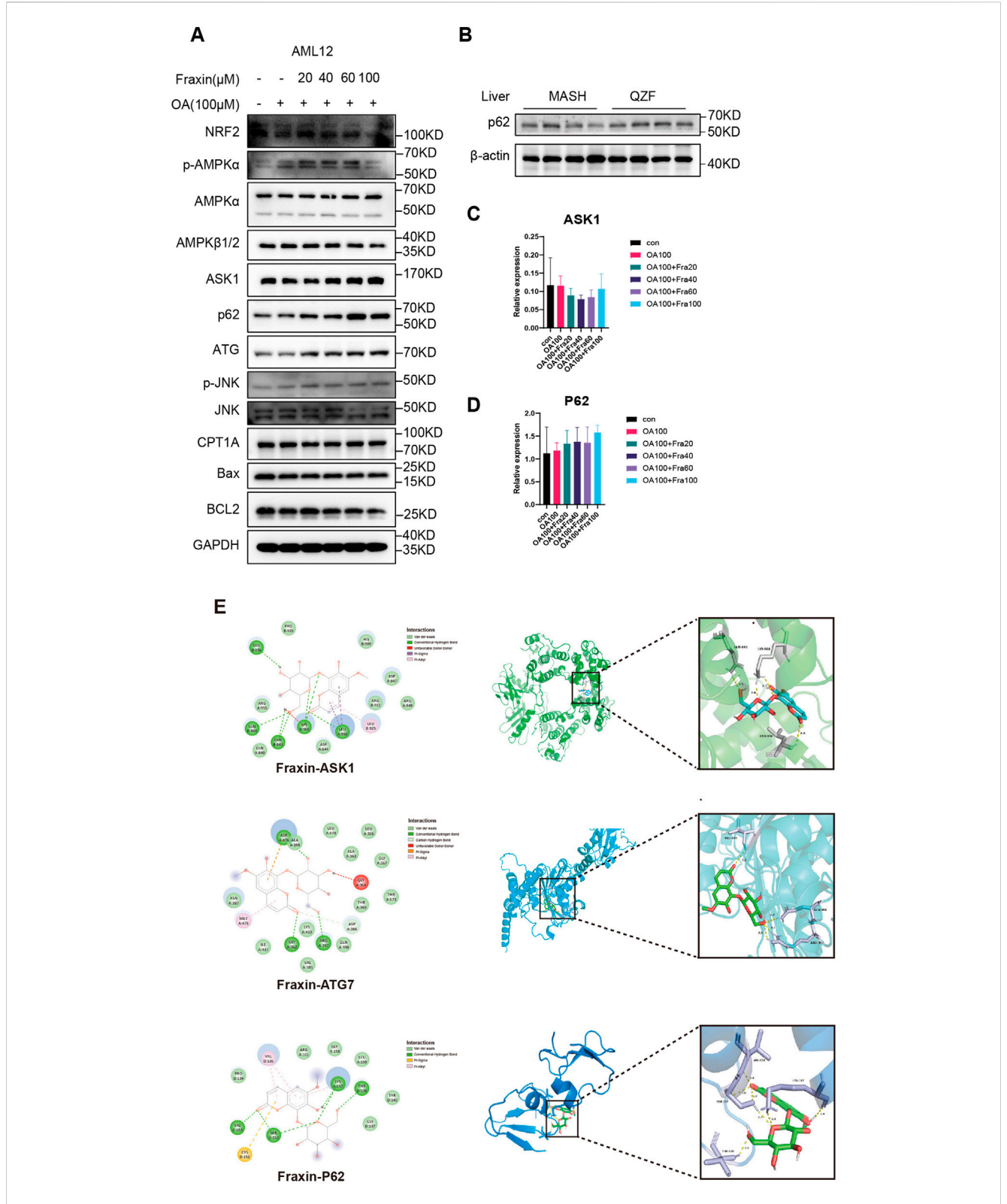
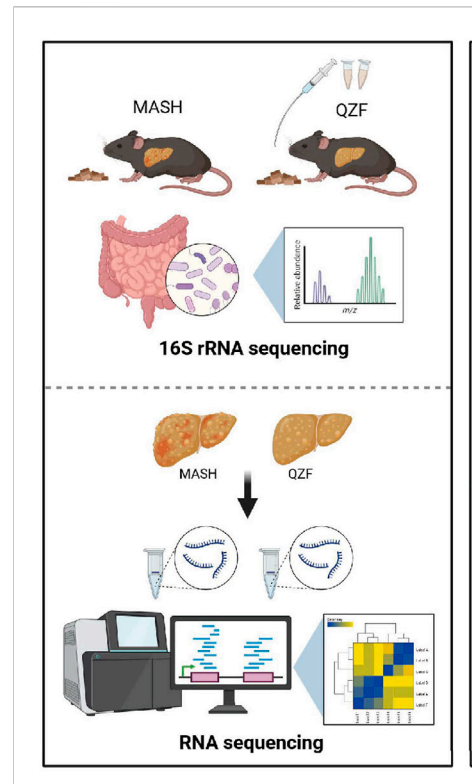
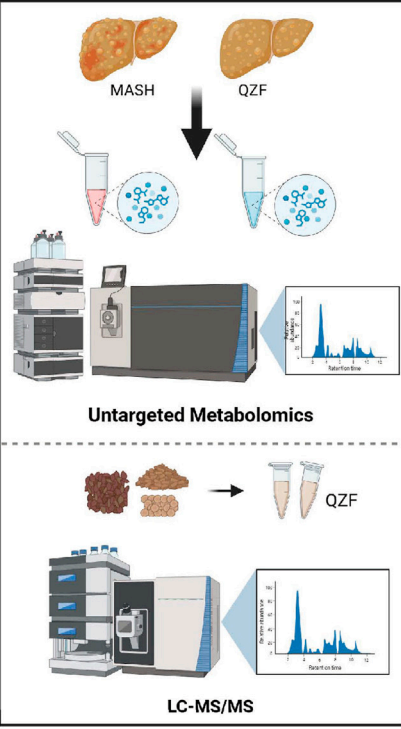
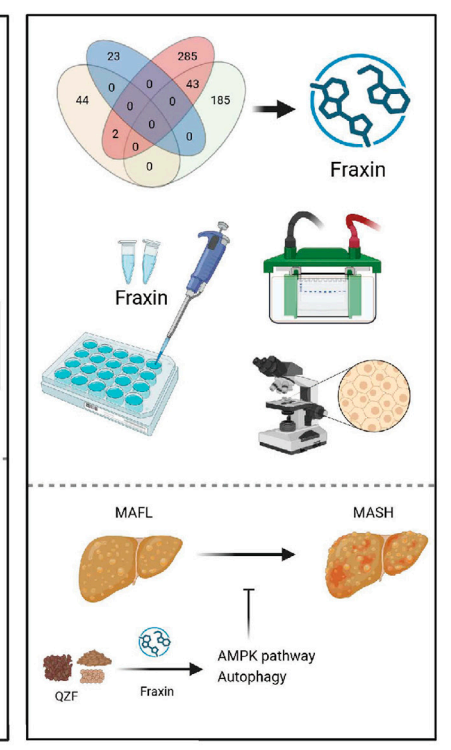


FIGURE 9
Fraxin ameliorates hepatic steatosis via AMPK-autophagy activation. (A) Western blot detection of AMPK-autophagy pathway related protein in Fraxin treated AML12 cell. (B) Western blot detection of P62 protein in QZF treated mice liver samples (n = 4). (C,D) qPCR detection of AMPK-autophagy pathway related genes in Fraxin treated AML12 cell. (E) Molecular docking analyse of Fraxin with AMPK-autophagy pathway related protein.







- Quzhi Formula Remodeled Gut Microbiota Composition and modulated Hepatic Transcriotome in MASH Mice
- Quzhi Formula Altered Hepatic
 Metabolites Profiles in MASH;
 Identification the potential active
 pharmaceutical ingredients of QZF by LC MS/MS
- Quzhi Formula actived AMPK pathway and induced autophagy to improve MASH with Fraxin

Graphical summary of the study. QZF decoction alleviates MASH by modulating gut microbiota, lipid metabolism, and Fraxin-driven autophagy. This graphical summary was generated by BioRender (https://biorender.com/).

toxicity or histopathological damage to vital organs (Supplementary Figure S3), thereby supporting its safety profile.

To investigate the impact of QZF on gut microbial diversity in MASH, we conducted 16S rRNA sequencing of fecal samples. The α -diversity analysis showed a significant increase in microbial richness and evenness following treatment, indicating a restoration of gut microbial homeostasis (Supplementary Figure S4). Principal coordinate analysis further revealed that the microbial community structure in the QZF-treated group was markedly separated from that of the MASH model group (Figures 2A,B). To investigate the shared and unique bacterial taxa among the three experimental groups (Control, MASH, and QZF), we performed OTU-based comparative analyses using both Venn and UpSet plots. A total of 149 OTUs were commonly shared across all three groups, representing a core microbial community. Group Control exhibited the highest number of unique OTUs (n = 195), followed by group QZF (n = 49) and group MASH (n = 21), suggesting substantial group-specific microbial signatures.

In addition to these unique taxa, 34 OTUs were found to be shared exclusively between groups Control and QZF, and 10 OTUs were shared between groups Control and MASH. Notably, 102 OTUs were shared between groups QZF and MASH but were absent in group Control, indicating potential similarities in microbial composition or response patterns between these two groups (Figures 2C,D).

To assess microbial richness and complexity, alpha diversity was evaluated across the three groups using observed OTU counts $\frac{1}{2}$

(Figure 2E). Further analysis of genus-level microbial composition revealed several taxa associated with NAFLD progression (Figure 2F). Notably, the relative abundance of *Enterococcus* was markedly elevated in group MASH compared to groups Control and QZF. In contrast, the abundance of *Enterococcus* was relatively suppressed in group QZF, suggesting a potential protective effect of the intervention applied in this group. These results collectively highlight both the conserved and distinct metabolites of the gut microbiota under different conditions.

The PCoA of the microbiota revealed that, while the microbial community in the QZF treatment group was distinct from that of the MASH group, it remained more similar to the MASH group than to the control. This indicates that the amelioration of MASH by QZF is only partially mediated by remodeling the gut microbiota, suggesting that other mechanisms, such as those involving metabolic regulation, are also likely involved.

3.2 QZF modulates hepatic transcriptome and activates AMPK/autophagy-related metabolic pathways

To reveal the potential mechanism of QZF on MASH, the RNA-seq analysis of liver tissue was performed. Based on the trend of gene changes in the MASH and QZF treatment groups, we further

categorized the gene profiles into eight groups (Figure 3A). Genetic profiles 2 and 5 were the focus of our attention. This is because the results showed that the transcriptional profiles were converted to the expression profiles of normal mice after treatment with the QZF (Figure 3B). Further, the GO and KEGG analysis enriched in metabolic pathways (Figures 3C,D). Gene Set Enrichment Analysis (GSEA) revealed that the gene set associated with positive regulation of autophagy and AMPK signaling pathway were enriched in the experimental group (Figures 3E,F).

3.3 QZF alters hepatic metabolites profiles in MASH

To investigate global metabolic alterations, untargeted metabolomics analysis was performed in liver tissues in both positive and negative ion modes. In both ion modes, the Control group clustered tightly on the left side of the PCA space, while MASH samples were clearly separated along the first principal metabolite (PC1), indicating significant metabolic disorder. Notably, samples from the QZF-treated group formed a distinct cluster that partially overlapped with the MASH group but shifted toward the Control group, suggesting a partial metabolic restoration upon QZF treatment (Figure 4A). Heatmaps of sample-to-sample Pearson correlation coefficients revealed high intra-group consistency and distinct inter-group separations. Samples within the Control, MASH, and QZF-treated groups exhibited strong internal correlations, while clear dissimilarities were observed between groups. The QZF group showed moderate similarity to MASH and partial separation, suggesting a metabolic shift upon treatment (Figure 4B). To further explore group-specific metabolic alterations, orthogonal partial least squares discriminant analysis (OPLS-DA) was performed under positive ion mode (Figures 4C,D). Clear metabolic separation was observed between the Control and MASH groups in both OPLS-DA score plots. Similarly, OPLS-DA demonstrated clear separation between the MASH and QZF-treated groups, suggesting significant metabolic remodeling after treatment.

A total of 231 significantly altered metabolites (73 upregulated and 158 downregulated) were identified in the Control vs. MASH comparison under positive mode, reflecting profound metabolic disruptions in the MASH group. In contrast, only 39 differential metabolites were found between the MASH and QZF groups, suggesting partial metabolic normalization following QZF treatment (Figures 5A–C). Pathway enrichment analysis identified a series of differentially enriched metabolites, highlighting the important involvement of metabolic pathways, such as lipid metabolism, amino acid metabolism, and purine metabolism (Figures 5D–G).

3.4 LC-MS/MS-metabolomics integration reveals QZF's bioactive metabolites and Anti-MASH mechanisms

Multivariate trajectory analysis of the hepatic metabolome revealed eight characteristic response patterns to MASH pathogenesis and QZF treatment (Figure 6A). Clusters 2 and 5 were identified as critical regulatory modules through therapeutic efficacy weighting algorithms, demonstrating complete metabolic reprogramming toward physiological steady-state conditions post-intervention (Figure 6B; Supplementary Table S3). Specifically, Profile 2 clustering patterns revealed that its KEGG pathway classification was mainly focused on metabolic pathways, and further analysis showed the enrichment of autophagy-inducing metabolites and mecrobial metabolism after treatment, suggesting activation of protective metabolic programs (Figures 6C,D).

To identify candidate bioactive metabolites responsible for the therapeutic effects of QZF, LC-MS-based metabolic profiling was performed on the QZF extract, there were total 223 active metabolites were identified (Supplementary Table S1).

A Venn diagram analysis was conducted to compare the metabolites detected in QZF with those found in the biological samples from Profile2 and Profile5. The analysis revealed that one metabolite—Fraxin—overlapped between these groups (Figure 7A). This overlap suggests that this metabolite may be systemically absorbed and functionally active in the biological context.

Fraxin, a glycoside exhibiting antioxidant and antiinflammatory activities (Figure 7B), was the focus of this investigation. It was consistently detected in both QZF and animal liver. Its retention time matched well with a major peak in the QZF chromatogram, supporting its identity and abundance (Figures 7C,D). These findings suggest that Fraxin may serve as a candidate bioactive metabolite contributing to the observed therapeutic effects of QZF.

3.5 Fraxin ameliorates hepatic steatosis via AMPK-autophagy activation

To assess the safety of Fraxin, cell viability assays were conducted on AML12 hepatocytes treated with increasing concentrations of Fraxin. And no significant cytotoxicity was observed across all doses, indicating a favorable safety profile (Figure 8A). Next, the lipid-lowering effect of Fraxin was evaluated using a free fatty acid (FFA)-induced steatosis model in HepG2 cells and AML12 cells. Enzymatic biochemical quantification of cellular lysates revealed that total cholesterol (TC) and triglyceride (TG) levels were significantly decreased following Fraxin treatment (Figure 8B). Moreover, BODIPY staining revealed massive intracellular lipid droplet accumulation in the FFA group, which was substantially reduced by Fraxin in a dose-dependent manner (Figure 8C). Notably, treatment with Fraxin at 60 µM almost completely abolished lipid accumulation, with effects comparable to the positive control Resmetirom. Oil Red O staining showed a marked reduction in lipid droplet accumulation in the treatment group compared to the Control group, indicating effective amelioration of hepatic steatosis (Figure 8D). These findings suggest that Fraxin effectively attenuates hepatic lipid accumulation in vitro, supporting its potential as a therapeutic agent for MAFLD.

To elucidate the mechanism by which Fraxin alleviates lipid accumulation, key signaling proteins were analyzed by Western blot in OA-induced AML12 cells. Fraxin dose-dependently increased the expression of NRF2, phosphorylation of AMPK α and total AMPK α , indicating activation of the AMPK pathway. Fraxin treatment also elevated Autophagy-related proteins ATG7, ASK1, and

phosphorylated JNK (p-JNK). Additionally, P62 expression increased in both *in vitro* (AML12 cells) and *in vivo* (liver tissue from QZF-treated mice) (Figures 9A,B). and no significant change was observed in expression of pro-apoptotic proteins such as Bax. qPCR assay showed that Fraxin treatment did not significantly affect the transcript levels of ASK1 and P62, suggesting that Fraxin may play a role through post-translational regulation (Figures 9C,D).

Following GSEA of RNA-seq data that suggested QZF-induced upregulation of autophagy pathways, the molecular interactions between Fraxin and a pivotal autophagy-associated protein were investigated *in silico* using molecular docking simulations. Molecular docking revealed significant binding affinities between Fraxin and key autophagy-related proteins ASK1, ATG7, and P62. As depicted in Figure 9E, the most stable complexes, indicated by their binding free energies, were Fraxin-ASK1 (–8.3 kcal/mol), Fraxin-ATG7 (–7.5 kcal/mol), and Fraxin-P62 (–6.3 kcal/mol).

These findings collectively support that Fraxin exerts its hepatoprotective effect by activating AMPK signaling, enhancing autophagy, and suppressing oxidative stress and apoptosis.

4 Discussion

Metabolic dysfunction-associated steatohepatitis (MASH) represents a multifactorial global health challenge. Current clinical treatments for MASH demonstrate limited efficacy and frequently cause significant adverse effects (Tang et al., 2025). In this study, we demonstrated that QZF alleviates metabolic dysfunction-associated steatohepatitis (MASH) coordinated multi-system modulation. The gut-liver emerged as a pivotal therapeutic target, evidenced by the QZFinduced recovery of microbial diversity and suppression of prosteatotic genera such as Enterococcus. Gut microbiota dysbiosis is closely associated with the pathogenesis of MASH. Although current studies on gut microbial composition in MASH patients and animal models yield inconsistent results, a consensus exists that at the phylum level, MAFLD patients exhibit reduced Bacteroidetes alongside increased Firmicutes and Proteobacteria (Aron-Wisnewsky et al., 2020). At the family level, Rikenellaceae is diminished while Enterobacteriaceae is elevated (Aron-Wisnewsky et al., 2020). At the genus level, Anaerobacterium, Coprococcus, Eubacterium, Faecalibacterium, and Prevotella are decreased, whereas Escherichia, Dorea, and Peptoniphilus are significantly enriched (Boursier et al., 2016). Elevated abundance of Gram-negative bacteria in the gut-such as Enterobacter, Escherichia, and Shigella-has been implicated in MASH development (Frost et al., 2021). These Gram-negative bacteria release lipopolysaccharides (LPS) through lysis, which disrupts the host's intestinal epithelial barrier. In obese individuals with fatty liver and high-fat diet-fed mice, gut microbiota analysis reveals increased proportions of Firmicutes (e.g., Dorea, Lactobacillus, Lachnospiraceae, and Clostridioides) (Le Roy et al., 2013; Raman et al., 2013). Notably, Firmicutes exhibit high metabolic efficiency in energy extraction during dietary degradation (Michail et al., 2015). Additionally, elevated levels of Erysipelotrichaceae are observed in the gut microbiota of low-choline diet-fed fatty liver patients and methionine-choline-deficient (MCD) diet-fed Erysipelotrichaceae exacerbates hepatic toxicity by converting choline into methylamines, thereby reducing host choline bioavailability and impairing hepatic secretion of very-lowdensity lipoprotein (VLDL), ultimately contributing to liver injury (Chen et al., 2020). In this study, the relative abundance of Enterococcus was markedly elevated in CDAHFD diet-fed mice, which were notably suppressed by QZF. It has been reported that a significant overrepresentation of Enterococcus spp. in pediatric cohorts with concurrent obesity and NAFLD (Wei et al., 2024). Enterococcus faecium B6 (Enterococcus faecium B6) could synthesize tyramine, a bioactive metabolite implicated in PPAR-y activation, thereby driving transcriptional cascades linked to hepatic lipid deposition, inflammatory infiltration, and fibrogenesis (Wei et al., 2024). We also observed that the model group clustered closely with the QZF group but remained distant from the normal group. The proximity between the Model and QZF groups in the PCA plot implies that QZF treatment did not fully restore the gut microbiota structure to that of the Normal group. This suggests that QZF may exert its therapeutic effects not solely by normalizing the microbiota, but also through other mechanisms such as modulating metabolic pathways.

Importantly, untargeted metabolomics revealed the activation of autophagy-associated metabolic pathways, suggesting that QZF reprograms the hepatic metabolic environment toward a protective state. This was further supported by RNA-seq findings, which uncovered upregulation of proteins involved in autophagy, lipid transport, and oxidative stress response. Autophagy, a conserved intracellular degradation pathway for organelles and proteins, encompasses three distinct subtypes: microautophagy, chaperone-mediated autophagy, and macroautophagy (Mizushima and Komatsu, 2011). These processes collectively maintain cellular homeostasis by delivering degradation substrates to lysosomes for proteolytic recycling (Fujiwara et al., 2013). Autophagy exhibits substrate diversity in cellular metabolite degradation: beyond proteolysis to replenish free amino acids, it facilitates the mobilization and hydrolysis of stored lipids and glycogen (Leung et al., 2016; Ezaki et al., 2011). Selective subtypes—including mitophagy (mitochondrial autophagy), reticulophagy (endoplasmic reticulum autophagy), and pexophagy (peroxisomal autophagy)-precisely regulate the quantity and functionality of these organelles (Singh et al., 2009; Kuma et al., 2004). Furthermore, autophagy mediates the selective degradation of enzymes and proteins involved in glycolysis, lipophagy, and catabolic pathways, thereby modulating the activity of these metabolic cascades (Cecco et al., 2008). Through these multifaceted mechanisms, autophagy engages in hepatic metabolic regulation, underpinning its critical role in diverse liver pathologies, particularly MASH (Hazari et al., 2020). Notably, metabolic syndrome-associated pathological features—including obesity, hyperglycemia, and dyslipidemia-exert deleterious effects on autophagic flux. Hepatic insulin resistance and lipid overload disrupt autophagic-lysosomal function, manifesting as impaired lipid clearance and sustained endoplasmic reticulum stress (ERS) (Liu et al., 2009). Conversely, autophagy deficiency exacerbates insulin resistance, ERS, and lipid metabolic dysregulation, establishing a mutually reinforcing pathological loop between autophagic dysfunction and MAFLD that accelerates MASH progression (Rodriguez-Navarro et al., 2012; Koga et al., 2010). These findings underscore autophagy's

pleiotropic role in MASH pathogenesis and highlight the therapeutic potential of enhancing hepatocyte-specific autophagic activity for MASH amelioration.

Histological analysis confirmed the functional outcomes of these molecular changes, as evidenced by reduced lipid droplet accumulation and significant improvements in serum lipid profiles. Taken together, these results suggest that QZF exerts a multi-faceted effect on MASH pathophysiology, involving microbiome reshaping, metabolic reprogramming, and autophagy induction. Moreover, the integration of multi-omics data highlights the potential of QZF as a systems-level therapy for complex metabolic disorders like MASH.

A key limitation of this study is the relatively high dose of QZF required to achieve therapeutic efficacy, a common challenge in phytopharmacology due to the low concentration of active principles. This is directly attributable to the nature of the crude extract used, where the bioactive metabolite(s) are present in low abundance. It is important to note that while interspecies dose conversion based on body surface area is a valid approach for drugs with low human starting doses (Reagan-Shaw et al., 2008; Xu et al., 2002), its applicability diminishes for high-dose preparations, such as traditional botanical drugs decoctions. The resulting concentrations in animal models can become pharmacologically problematic and prone to artifacts, a concern highlighted in a recent consensus statement (Zhan et al., 2019). Consequently, future research will prioritize the bioactivity-guided fractionation and purification of the active metabolites from QZF. This strategy is essential to achieve potent therapeutic effects at substantially lower, pharmacologically conventional doses, which will not only enhance translational potential but also provide a clearer elucidation of the precise molecular mechanisms of action.

Our findings demonstrate that Fraxin ameliorates hepatic steatosis and exerts hepatoprotective effects through a multimechanistic framework involving AMPK signaling activation, autophagy enhancement, and suppression of oxidative stress and apoptosis. These results align with prior evidence showing Fraxin's capacity to mitigate CCl4-induced liver injury via inhibition of MAPK/NF-kB-mediated oxidative stress, lipid peroxidation, and inflammatory cascades (Niu et al., 2017), further solidifying its therapeutic potential for hepatic pathologies. Importantly, as a principal bioactive metabolite of the QZF, Fraxin's autophagymodulating properties may underpin QZF's systemic efficacy in MASH. However, the precise interplay between Fraxin-mediated AMPK activation and downstream autophagic flux regulation warrants further mechanistic dissection, particularly in the context of lipid droplet clearance and inflammasome resolution. Future studies should prioritize dose-dependent efficacy profiling, off-target effect assessments, and clinical validation of Fraxin's therapeutic index. Additionally, mechanistic investigations into its role within QZF's phytochemical network could uncover novel combinatorial strategies for treating multifactorial hepatic disorders.

This study demonstrates that QZF ameliorates MASH through multi-system regulation, primarily targeting the gut-liver axis by restoring microbial diversity, suppressing pro-steatotic *Enterococcus*, and activating AMPK/Autophagy-associated pathways to reprogram hepatic metabolism through active metabolite Fraxin. Integrated multi-omics and histological analyses confirm QZF's efficacy in reducing lipid accumulation,

improving serum lipid profiles, and inducing protective molecular mechanisms, positioning it as a systems-level therapeutic candidate for complex metabolic disorders (Figure 10).

Data availability statement

The data presented in the study are deposited in the National Genomics Data Center (NGDC) repository, accession number CRA026321. Any other data are available from the corresponding author on reasonable request.

Ethics statement

The animal studies were approved by the Institutional Animal Ethics Review Board at Shanghai Jiao Tong University. The studies were conducted in accordance with the local legislation and institutional requirements. Written informed consent was obtained from the owners for the participation of their animals in this study.

Author contributions

JW: Writing – review and editing, Data curation, Formal Analysis, Funding acquisition, Writing – original draft. YW: Data curation, Formal Analysis, Writing – original draft. ML: Investigation, Writing – review and editing. YL: Data curation, Writing – review and editing. YH: Formal Analysis, Writing – review and editing. YG: Formal Analysis, Writing – review and editing. XW: Formal Analysis, Writing – review and editing. HC: Data curation, Writing – review and editing. JX: Formal Analysis, Writing – review and editing. Writing – review and editing. TS: Formal Analysis, Writing – review and editing. TS: Funding acquisition, Investigation, Writing – review and editing. TS: Funding acquisition, Project administration, Supervision, Writing – original draft, Writing – review and editing. OZ: Conceptualization, Funding acquisition, Supervision, Writing – original draft, Writing – review and editing.

Funding

The author(s) declare that financial support was received for the research and/or publication of this article. This research was supported by National Natural Science Foundation of China (82300971), the Fundamental Research Funds for the Central Universities (YG2022QN116), the National Key Research and Development Program of China (2021YFC2701900, 2021YFC2701903), the Research Fund of Shanghai Tongren Hospital, Shanghai Jiaotong University School of Medicine (TRKYRC-xx202212, TRYJ2022LC03, TR2014rc03), the Research Fund of Health Commission of Jing'an District (2024QT02).

Acknowledgments

We are grateful to Guangzhou Genedenovo Biotechnology Co., Ltd., for assisting in sequencing, metabolite and bioinformatics analysis.

Conflict of interest

The authors declare that the research was conducted in the absence of any commercial or financial relationships that could be construed as a potential conflict of interest.

Generative AI statement

The author(s) declare that no Generative AI was used in the creation of this manuscript.

Any alternative text (alt text) provided alongside figures in this article has been generated by Frontiers with the support of artificial intelligence and reasonable efforts have been made to ensure accuracy, including review by the authors wherever possible. If you identify any issues, please contact us.

Publisher's note

All claims expressed in this article are solely those of the authors and do not necessarily represent those of their affiliated organizations, or those of the publisher, the editors and the reviewers. Any product that may be evaluated in this article, or claim that may be made by its manufacturer, is not guaranteed or endorsed by the publisher.

Supplementary material

The Supplementary Material for this article can be found online at: https://www.frontiersin.org/articles/10.3389/fphar.2025.1694242/full#supplementary-material

SUPPLEMENTARY FIGURE \$1

The LC-MS fingerprint of the QZF extract. (A) The LC-MS fingerprint of QZF extract in both ion mode showed good instrument precision, with RSDs of

relative retention time and peak area at 0.00%–0.22% and 1.06%–1.43%, respectively. The cosine similarity algorithm was used to assess similarity between samples and common peaks, both overall and within sample groups. (B) Metabolites identified in QZF extract were marked by number.

SUPPLEMENTARY FIGURE S2

The low dosage of QZF (4.1666 g/kg) did not alleviate hepatic steatosis in a MASH mouse model. Male C57BL/6 SPF mice (6 weeks old) were fed a CDAHFD for 3 weeks to induce MASH, followed by daily oral gavage of either the low-dose QZF (4.1666 g/kg) or a PBS vehicle for an additional 4 weeks. Mice were euthanized at the end of week 7 for liver collection. Representative liver sections stained with (A) H θ E and (B) Oil Red O are shown. Graphs depict the NAFLD Activity Score (NAS) and the semi-quantitative analysis of lipid deposition from Oil Red O staining, performed using ImageJ. **p < 0.01, ***p < 0.001, ****p < 0.0001 vs. model group (one-way ANOVA). Abbreviations: MASH, metabolic dysfunction-associated steatohepatitis; CDAHFD, choline-deficient, L-amino acid-defined, high-fat diet; H θ E, hematoxylin and eosin.

SUPPLEMENTARY FIGURE S3

Acute toxicity assessment of the high-dose QZF in mice. A separate acute toxicity study was conducted to evaluate the safety of QZF. Male C57BL/6 SPF mice (6 weeks old) received a daily oral gavage of QZF at 8.3331 g/kg or PBS vehicle for 4 weeks. (A) Representative gross images of the liver. (B) Serum levels of alanine aminotransferase (ALT) and aspartate aminotransferase (AST). (C–F) Representative histopathological images of H&E-stained sections from the liver (C), kidney (D), heart (E), and lung (F). Data are presented as mean \pm SD (n = 9). **p < 0.01, ***p < 0.001, ****p < 0.0001 vs. PBS control group (unpaired two-tailed Student's t-test).

SUPPLEMENTARY FIGURE \$4

The α -diversity analysis. Fecal samples were collected immediately after sacrifice from mice treated with the QZF and from normal controls. Subsequently, 16S rRNA sequencing was performed on these samples. The resulting alpha diversity indices—Shannon (A), Simpson (B), Chao (C), and ACE (D)—for both groups and individual samples are presented in this figure.

SUPPLEMENTARY TABLE S1

Active metabolites of QZF decoction.

SUPPLEMENTARY TABLE S2

ConPhyMP-checklist.

SUPPLEMENTARY TABLE S3

Liver metabolites after QZF treated.

References

Aron-Wisnewsky, J., Vigliotti, C., Witjes, J., Le, P., Holleboom, A. G., Verheij, J., et al. (2020). Gut microbiota and human NAFLD: disentangling microbial signatures from metabolic disorders. *Nat. Rev. Gastroenterol. Hepatol.* 17 (5), 279–297. doi:10.1038/s41575-020-0269-9

Boursier, J., Mueller, O., Barret, M., Machado, M., Fizanne, L., Araujo-Perez, F., et al. (2016). The severity of nonalcoholic fatty liver disease is associated with gut dysbiosis and shift in the metabolic function of the gut microbiota. *Hepatology* 63 (3), 764–775. doi:10.1002/hep.28356

Buzzetti, E., Pinzani, M., and Tsochatzis, E. A. (2016). The multiple-hit pathogenesis of non-alcoholic fatty liver disease (NAFLD). *Metabolism* 65 (8), 1038–1048. doi:10. 1016/j.metabol.2015.12.012

Cecconi, F., and Levine, B. (2008). The role of autophagy in mammalian development: cell makeover rather than cell death. *Dev. Cell* 15 (3), 344–357. doi:10.1016/j.devcel. 2008.08.012

Chai, H., Shen, T., Liu, Y., Yin, R., Wu, Z., Wu, Y., et al. (2020). Mechanisms of quzhisanwei formula for non-alcoholic steatohepatitis based on a network pharmacology approach. *Med. Data Min.* 3, 92–101. doi:10.53388/mdm2020063005

Chen, J., and Vitetta, L. (2020). Gut microbiota metabolites in NAFLD pathogenesis and therapeutic implications. *Int. J. Mol. Sci.* 21 (15), 5214. doi:10.3390/ijms21155214

Dehghani, S., Mehri, S., and Hosseinzadeh, H. (2019). The effects of Crataegus pinnatifida (Chinese hawthorn) on metabolic syndrome: a review. *Iran. J. Basic Med. Sci.* 22 (5), 460–468. doi:10.22038/ijbms.2019.31964.7678

Ezaki, J., Matsumoto, N., Takeda-Ezaki, M., Komatsu, M., Takahashi, K., Hiraoka, Y., et al. (2011). Liver autophagy contributes to the maintenance of blood glucose and amino acid levels. *Autophagy* 7 (7), 727–736. doi:10.4161/auto.7.7.15371

Fan, X., Hong, T., Yang, Q., Wang, D., Peng, J., Xiao, W., et al. (2022). Quality assessment of fried licorice based on fingerprints and chemometrics. *Food Chem.* 378, 132121. doi:10.1016/j.foodchem.2022.132121

Frost, F., Kacprowski, T., Rühlemann, M., Pietzner, M., Bang, C., Franke, A., et al. (2021). Long-term instability of the intestinal microbiome is associated with metabolic liver disease, low microbiota diversity, diabetes mellitus and impaired exocrine pancreatic function. *Gut* 70 (3), 522–530. doi:10.1136/gutjnl-2020-322753

Fujiwara, Y., Furuta, A., Kikuchi, H., Aizawa, S., Hatanaka, Y., Konya, C., et al. (2013). Discovery of a novel type of autophagy targeting RNA. *Autophagy* 9 (3), 403–409. doi:10.4161/auto.23002

Gong, L., Wang, G.-E., Ma, Q.-Y., Hao, W.-Z., Xian, M.-H., Wu, Y.-P., et al. (2022). Novel insights into the effect of xiaoyao san on corticosterone-induced hepatic steatosis: inhibition of glucocorticoid receptor/perilipin-2 signaling pathway. *Acupunct. Herb. Med.* 2 (1), 49–57. doi:10.1097/hm9.00000000000011

Hagström, H., Shang, Y., Hegmar, H., and Nasr, P. (2024). Natural history and progression of metabolic dysfunction-associated steatotic liver disease. *Lancet Gastroenterol. Hepatol.* 9 (10), 944–956. doi:10.1016/s2468-1253(24)00193-6

Hazari, Y., Bravo-San Pedro, J. M., Hetz, C., Galluzzi, L., and Kroemer, G. (2020). Autophagy in hepatic adaptation to stress. *J. Hepatol.* 72 (1), 183–196. doi:10.1016/j. jhep.2019.08.026

Jarvis, H., Craig, D., Barker, R., Spiers, G., Stow, D., Anstee, Q. M., et al. (2020). Metabolic risk factors and incident advanced liver disease in non-alcoholic fatty liver disease (NAFLD): a systematic review and meta-analysis of population-based observational studies. *PLoS Med.* 17 (4), e1003100. doi:10.1371/journal.pmed. 1003100

Koga, H., Kaushik, S., and Cuervo, A. M. (2010). Altered lipid content inhibits autophagic vesicular fusion. Faseb J. 24 (8), 3052–3065. doi:10.1096/fj.09-144519

Kokkorakis, M., Boutari, C., Hill, M. A., Kotsis, V., Loomba, R., Sanyal, A. J., et al. (2024). Resmetirom, the first approved drug for the management of metabolic dysfunction-associated steatohepatitis: trials, opportunities, and challenges. *Metabolism* 154, 155835. doi:10.1016/j.metabol.2024.155835

Kuchay, M. S., Choudhary, N. S., and Mishra, S. K. (2020). Pathophysiological mechanisms underlying MAFLD. *Diabetes Metab. Syndr.* 14 (6), 1875–1887. doi:10. 1016/j.dsx.2020.09.026

Kuma, A., Hatano, M., Matsui, M., Yamamoto, A., Nakaya, H., Yoshimori, T., et al. (2004). The role of autophagy during the early neonatal starvation period. *Nature* 432 (7020), 1032–1036. doi:10.1038/nature03029

Le Roy, T., Llopis, M., Lepage, P., Bruneau, A., Rabot, S., Bevilacqua, C., et al. (2013). Intestinal microbiota determines development of non-alcoholic fatty liver disease in mice. *Gut* 62 (12), 1787–1794. doi:10.1136/gutjnl-2012-303816

Leung, C., Rivera, L., Furness, J. B., and Angus, P. W. (2016). The role of the gut microbiota in NAFLD. *Nat. Rev. Gastroenterol. Hepatol.* 13 (7), 412–425. doi:10.1038/nrgastro.2016.85

Liang, S., Dong, Y., Chang, Z., Guo, P., Jia, J., Yang, G., et al. (2025). An integrative pharmacology-based study on the pharmacological activity and mechanism of xiaoji-chenpi formula (XCF) against MAFLD. *Front. Pharmacol.* 16, 1521111–1522025. doi:10.3389/fphar.2025.1521111

Liu, H. Y., Han, J., Cao, S. Y., Hong, T., Zhuo, D., Shi, J., et al. (2009). Hepatic autophagy is suppressed in the presence of insulin resistance and hyperinsulinemia: inhibition of FoxO1-dependent expression of key autophagy genes by insulin. *J. Biol. Chem.* 284 (45), 31484–31492. doi:10.1074/jbc.M109.033936

Miao, L., Targher, G., Byrne, C. D., Cao, Y. Y., and Zheng, M. H. (2024). Current status and future trends of the global burden of MASLD. *Trends Endocrinol. Metab.* 35 (8), 697–707. doi:10.1016/j.tem.2024.02.007

Michail, S., Lin, M., Frey, M. R., Fanter, R., Paliy, O., Hilbush, B., et al. (2015). Altered gut microbial energy and metabolism in children with non-alcoholic fatty liver disease. *FEMS Microbiol. Ecol.* 91 (2), 1–9. doi:10.1093/femsec/fiu002

Mizushima, N., and Komatsu, M. (2011). Autophagy: renovation of cells and tissues. Cell 147 (4), 728–741. doi:10.1016/j.cell.2011.10.026

Niu, X., Liu, F., Li, W., Zhi, W., Yao, Q., Zhao, J., et al. (2017). Hepatoprotective effect of fraxin against carbon tetrachloride-induced hepatotoxicity *in vitro* and *in vivo* through regulating hepatic antioxidant, inflammation response and the MAPK-NF-kB signaling pathway. *Biomed. Pharmacother.* 95, 1091–1102. doi:10.1016/j.biopha. 2017.09.029

Peng, W., Qin, R., Li, X., and Zhou, H. (2013). Botany, phytochemistry, pharmacology, and potential application of Polygonum cuspidatum sieb.et zucc.: a review. *J. Ethnopharmacol.* 148 (3), 729–745. doi:10.1016/j.jep.2013.05.007

Qu, Y.-L., Deng, C.-H., Luo, Q., Shang, X.-Y., Wu, J.-X., Shi, Y., et al. (2019). Arid1a regulates insulin sensitivity and lipid metabolism. *EBioMedicine* 42, 481–493. doi:10. 1016/j.ebiom.2019.03.021

Raman, M., Ahmed, I., Gillevet, P. M., Probert, C. S., Ratcliffe, N. M., Smith, S., et al. (2013). Fecal microbiome and volatile organic compound metabolome in Obese humans with nonalcoholic fatty liver disease. *Clin. Gastroenterol. Hepatol.* 11 (7), 868–75.e753. doi:10.1016/j.cgh.2013.02.015

Rao, G., Peng, X., Li, X., An, K., He, H., Fu, X., et al. (2023). Unmasking the enigma of lipid metabolism in metabolic dysfunction-associated steatotic liver disease: from mechanism to the clinic. *Front. Med.* 10, 1294267–2023. doi:10.3389/fmed.2023. 1294267

Reagan-Shaw, S., Nihal, M., and Ahmad, N. (2008). Dose translation from animal to human studies revisited. Faseb J. 22 (3), 659–661. doi:10.1096/fj.07-9574LSF

Ren, Q., Sun, Q., and Fu, J. (2024). Dysfunction of autophagy in high-fat diet-induced non-alcoholic fatty liver disease. *Autophagy* 20 (2), 221–241. doi:10.1080/15548627. 2023.2254191

Rodriguez-Navarro, J. A., Kaushik, S., Koga, H., Dall'armi, C., Shui, G., Wenk, M. R., et al. (2012). Inhibitory effect of dietary lipids on chaperone-mediated autophagy. *Proc. Natl. Acad. Sci. U S A.* 109 (12), E705–E714. doi:10.1073/pnas.1113036109

Singh, R., Kaushik, S., Wang, Y., Xiang, Y., Novak, I., Komatsu, M., et al. (2009). Autophagy regulates lipid metabolism. Nature~458~(7242),~1131-1135.~doi:10.1038/nature07976

Tamimi, A., Javid, M., Sedighi-Pirsaraei, N., and Mirdamadi, A. (2024). Exosome prospects in the diagnosis and treatment of non-alcoholic fatty liver disease. *Front. Med.* 11, 1420281–1422024. doi:10.3389/fmed.2024.1420281

Tang, Q., Yu, Q., Ni, B., Jiang, Z., and Zhang, L. (2024). Dual effects of psoraleae fructus on the liver: hepatoprotection or hepatoxicity? *Acupunct. Herb. Med.* 4 (2), 176–183. doi:10.1097/hm9.000000000000117

Tang, S., Yan, G., Kong, L., Sun, H., Liu, C., Han, Y., et al. (2025). Research progress on the hepatoprotective effect, pharmacokinetic properties, and hepatotoxicity of geniposide. *Acupunct. Herb. Med.* 5 (2), 136–146. doi:10.1097/hm9.0000000000000160

Wang, H., Liu, X., Wang, C., Yu, S., Yang, X., Cao, X., et al. (2025). Natural active botanical metabolites: targeting AMPK signaling pathway to treat metabolic dysfunction-associated fatty liver disease. *Front. Pharmacol.* 16, 1611400–1612025. doi:10.3389/fbhar.2025.1611400

Wei, J., Luo, J., Yang, F., Feng, X., Zeng, M., Dai, W., et al. (2024). Cultivated Enterococcus faecium B6 from children with obesity promotes nonalcoholic fatty liver disease by the bioactive metabolite tyramine. *Gut Microbes* 16 (1), 2351620. doi:10.1080/19490976.2024.2351620

Wong, V. W., Ekstedt, M., Wong, G. L., and Hagström, H. (2023). Changing epidemiology, global trends and implications for outcomes of NAFLD. *J. Hepatol.* 79 (3), 842–852. doi:10.1016/j.jhep.2023.04.036

Wu, J.-X., He, K.-Y., Zhang, Z.-Z., Qu, Y.-L., Su, X.-B., Shi, Y., et al. (2021). LZP is required for hepatic triacylglycerol transportation through maintaining apolipoprotein B stability. *PLoS Genet.* 17 (2), e1009357. doi:10.1371/journal.pgen.1009357

Wu, Y. L., Wu, J. X., Shen, T. T., Chai, H. S., Chen, H. F., and Zhang, Q. (2022). Quzhi formula alleviates nonalcoholic steatohepatitis by impairing hepatocyte lipid accumulation and inflammation via Bip/eIF2 α signaling. J. Clin. Transl. Hepatol. 10 (6), 1050–1058. doi:10.14218/jcth.2021.00458

Xie, P., Zhou, X., and Zhang, Q. (2010). Clinical observation of combined "Quzhi sanwei decoction" and warm acupuncture in treating 70 cases of fatty liver disease. *Shanghai J. Traditional Chin. Med.* 9, 3. doi:10.16305/j.1007-1334.2010.09.018

 $Xu,\,S.,\,Xu,\,S.\,S.,\,Bian,\,R.,\,Chen,\,X.,\,Rulian,\,K.,\,Xu,\,S.\,Y.,\,et\,al.$ (2002). Experimental methodology of pharmacology.

Xu, R., Wu, J., Pan, J., Zhang, S., Yang, Y., Zhang, L., et al. (2024). Gan-jiang-ling-zhu decoction improves steatohepatitis by regulating gut microbiota-mediated 12-tridecenoic acid inhibition. *Front. Pharmacol.* 15, 1444561–2024. doi:10.3389/fphar.2024.1444561

Yadav, J. P., Arya, V., Yadav, S., Panghal, M., Kumar, S., Dhankhar, S., et al. (2010). Cassia occidentalis L.: a review on its ethnobotany, phytochemical and pharmacological profile. *Fitoterapia* 81 (4), 223–230. doi:10.1016/j.fitote.2009.09.008

Younossi, Z., Anstee, Q. M., Marietti, M., Hardy, T., Henry, L., Eslam, M., et al. (2018). Global burden of NAFLD and NASH: trends, predictions, risk factors and prevention. *Nat. Rev. Gastroenterol. Hepatol.* 15 (1), 11–20. doi:10.1038/nrgastro.2017.109

Younossi, Z. M., Kalligeros, M., and Henry, L. (2025). Epidemiology of metabolic dysfunction-associated steatotic liver disease. *Clin. Mol. Hepatol.* 31 (Suppl. l), S32–s50. doi:10.3350/cmh.2024.0431

Zhan, T., Yao, N., Wu, L., Lu, Y., Liu, M., Liu, F., et al. (2019). The major effective components in shengmai formula interact with sodium taurocholate co-transporting polypeptide. *Phytomedicine* 59, 152916. doi:10.1016/j.phymed.2019.152916